Earth-Science Reviews 257 (2024) 104901

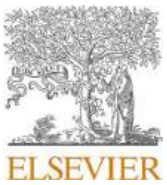

Contents lists available at ScienceDirect

Earth-Science Reviews

journal homepage: www.elsevier.com/locate/earscirev

Review Article

The uplift of the East Africa - Arabia swell

Andrea Sembroni [a,*], Claudio Faccenna [a,b], Thorsten W. Becker [c,d,e], Paola Molin [a]

[a] Department of Science, Roma Tre University, Rome, Italy
[b] GFZ, German Research Center for Geoscience, Germany
[c] Institute for Geophysics, Jackson School of Geosciences, The University of Texas at Austin, USA
[d] Department of Earth and Planetary Sciences, Jackson School of Geosciences, The University of Texas at Austin, USA
[e] Oden Institute for Computational Engineering & Sciences, The University of Texas at Austin, USA

ARTICLE INFO

Keywords:
Horn of Africa
Arabia
Afar superplume
Swell
Topography
Volcanism

ABSTRACT

The East Africa - Arabia topographic swell is an anomalously high-elevation region of ~4000 km long (from southern Ethiopia to Jordan) and ~ 1500 km wide (from Egypt to Saudi Arabia) extent. The swell is dissected by the Main Ethiopian, Red Sea, and Gulf of Aden rifts, and characterized by widespread basaltic volcanic deposits emplaced from the Eocene to the present. Geochemical and geophysical data confirm the involvement of mantle processes in swell formation; however, they have not been able to fully resolve some issues, e.g., regarding the number and location of plumes and uplift patterns. This study addresses these questions and provides a general evolutionary model of the region by focusing on the present topographic configuration through a quantitative analysis and correlating long and intermediate wavelength features with mantle and rifting processes. Moreover, the isostatic and dynamic components of topography have been evaluated considering a range of seismic tomographic models for the latter. When interpreted jointly with geological data including volcanic deposits, the constraints do imply causation by a single process which shaped the past and present topography of the study area: the upwelling of the Afar superplume. Once hot mantle material reached the base of the lithosphere below the Horn of Africa during the Late Eocene, the plume flowed laterally toward the Levant area guided by pre-existing discontinuities in the Early Miocene. Plume material reached the Anatolian Plateau in the Late Miocene after slab break-off and the consequent formation of a slab window. During plume material advance, buoyancy forces led to the formation of the topographic swell and tilting of the Arabia Peninsula. The persistence of mantle support beneath the study area for tens of million years also affected the formation and evolution of the Nile and Euphrates-Tigris fluvial networks. Subsequently, surface processes, tectonics, and volcanism partly modified the initial topography and shaped the present-day landscape.

1. Introduction

Earth's topography is the expression of the interactions between the floating equilibrium of a density column, surface processes, flexure, lithospheric deformation (i.e., tectonics, volcanism, and magmatic underplating), and mantle dynamics (e.g., Braun, 2010; Flament et al., 2013; Faccenna and Becker, 2020). To unravel some of these processes, the contributions to topography can be inferred as being due to two main components: the isostatic and dynamic ones (e.g., Panasyuk and Hager, 2000; Gvirtzman et al., 2016). The first depends on the heterogeneities in lithosphere structure and density; the second represents the deflection of the surface in response to mantle tractions arising from density driven flow in the mantle and plate motions. In particular, upwellings (i.e., mantle plumes), caused by the rise of hot mantle material, and downwellings, related to the descent of cold lithosphere during subduction, can cause uplift and subsidence at the surface, respectively (e.g., Hager et al., 1985; Panasyuk and Hager, 2000; Braun, 2010; Flament et al., 2013).

Mantle plumes show complex morphologies and dynamics (e.g. Heron, 2018; Koppers et al., 2021). One may classify them as "primary", consisting of whole-mantle structures rising from the core-mantle boundary as narrow, localized conduits or in the form of broader upwellings, or superplumes. "Secondary" plumes are confined to the upper mantle as the result of stagnation of the primary plumes at the base or within the mantle-transition zone (Ritsema et al., 1999; Courtillot et al., 2003; French and Romanowicz, 2015; Cloetingh et al., 2022). Regions

* Corresponding author.
E-mail address: andrea.sembroni@uniroma3.it (A. Sembroni).

https://doi.org/10.1016/j.earscirev.2024.104901
Received 15 February 2024; Received in revised form 10 August 2024; Accepted 15 August 2024
Available online 18 August 2024

affected by primary mantle plumes are often characterized by the emplacement of a huge volume of igneous rocks (Large Igneous Provinces – LIPs) typically attributed to the plume head arrival (e.g., Richards et al., 1989; Burke and Torsvik, 2004), and by broad, anomalously high-elevated regions (topographic swells; e.g. Richards et al., 1988; Ribe and Christensen, 1994; Heron, 2018). Despite successive isostatic adjustments and rifting events, topographic anomalies can be preserved for tens of millions of years by processes such as crustal thickening (McKenzie, 1984; Cox, 1989) and/or by the persistence of a mantle anomaly below the crust (Faccenna et al., 2019).

Topographic swells associated with mantle plumes are documented worldwide on both oceanic and continental plates (Dietz and Menard, 1953; Ribe and Christensen, 1994a, 1994b; Ribe and Christensen, 1999; Gurnis et al., 2000; Sengör, 2001; Daradich et al., 2003; Roberts and

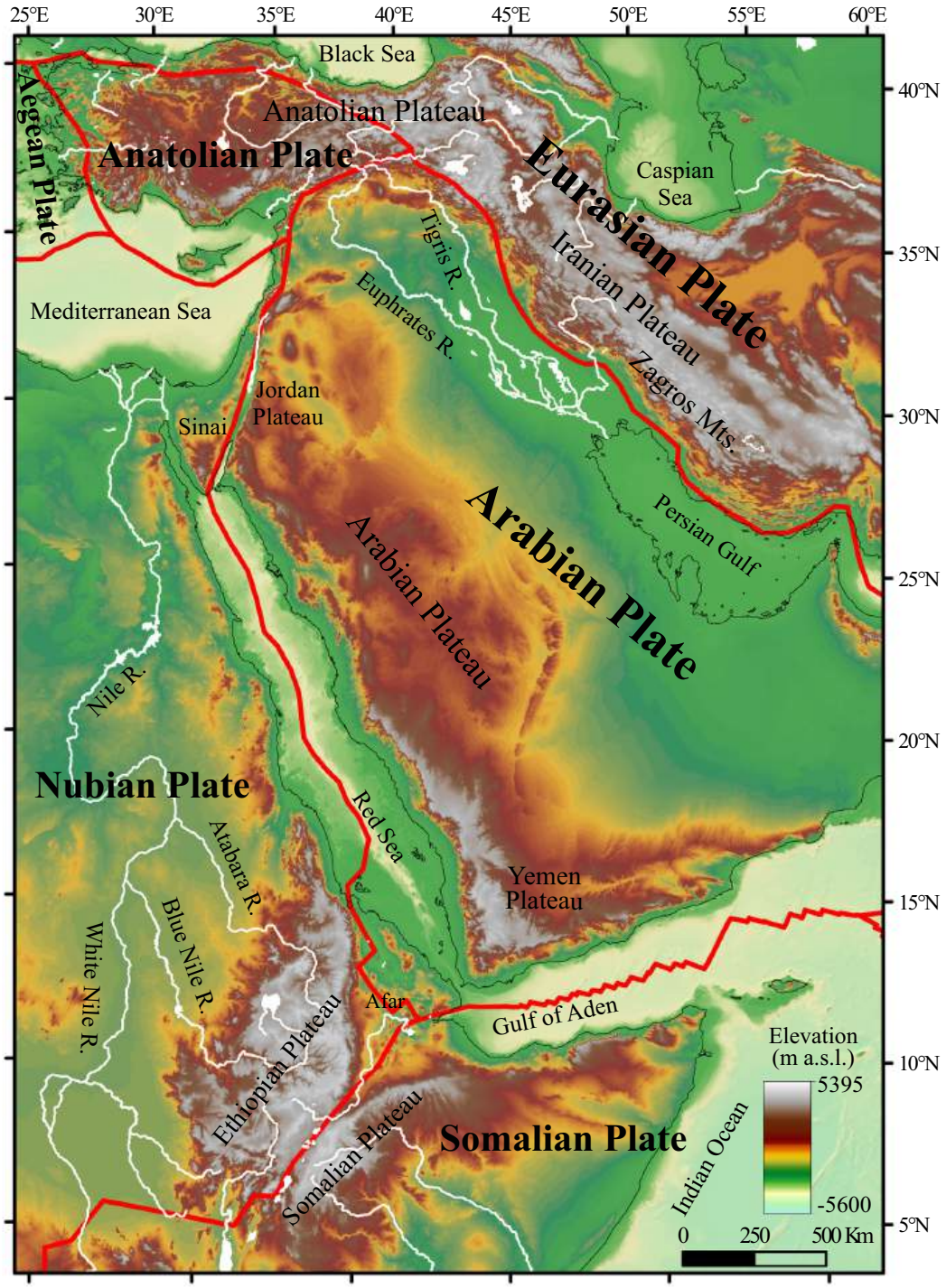

Fig. 1. Topographic configuration of the study area (ETOPO2022 global elevation model with resolution of ~500 m; www.ngdc.noaa.gov); the EAAS extends from south to north comprising the Ethiopian, Somalian, Arabian, and Jordan plateaux; solid red lines indicate plates boundaries. (For interpretation of the references to colour in this figure legend, the reader is referred to the web version of this article.)

White, 2010; Jones et al., 2012; Roberts et al., 2012; Davila and Lithgow-Bertelloni, 2013; Rowley et al., 2013; Czarnota et al., 2014; Paul et al., 2014; Liu, 2015; Heller and Liu, 2016; Sembroni et al., 2016a, 2021; Faccenna et al., 2019; Friedrich, 2019; Clementucci et al., 2023; Molin et al., 2023). Their formation and evolution has been addressed with numerical and analog convection models (e.g. Houseman, 1990; Griffiths and Campbell, 1991; Farnetani and Richards, 1994; Ribe and Christensen, 1994a, 1994b; Ribe and Christensen, 1999; d'Acremont et al., 2003; Burov and Guillou-Frottier, 2005; Moucha et al., 2008; Braun, 2010; Moucha and Forte, 2011; Crameri et al., 2012; Burov and Gerya, 2014; Koptev et al., 2015; Kiraly et al., 2015; Barnett-Moore et al., 2017; Koptev et al., 2017; Rubey et al., 2017; Sembroni et al., 2017; Cao et al., 2018).

One of the most studied ongoing swells is the East Africa-Arabia one (EAAS), also called the "Afro-Arabian dome" (Cloos, 1939; Almond, 1986; Camp and Roobol, 1992). It is an anomalously high-elevated region ~4000 km long (from southern Ethiopia to Jordan) and ~1500 km wide (from Egypt to Saudi Arabia; Cloos, 1939; Almond, 1986, Camp and Roobol, 1992; Avni et al., 2012; Bar et al., 2016; Fig. 1). The area is dissected by the Main Ethiopian, Red Sea, and Gulf of Aden rifts and is characterized, along its entire extent, by widespread volcanic deposits varying in age from Eocene to present-day (Coleman et al., 1983; Brown

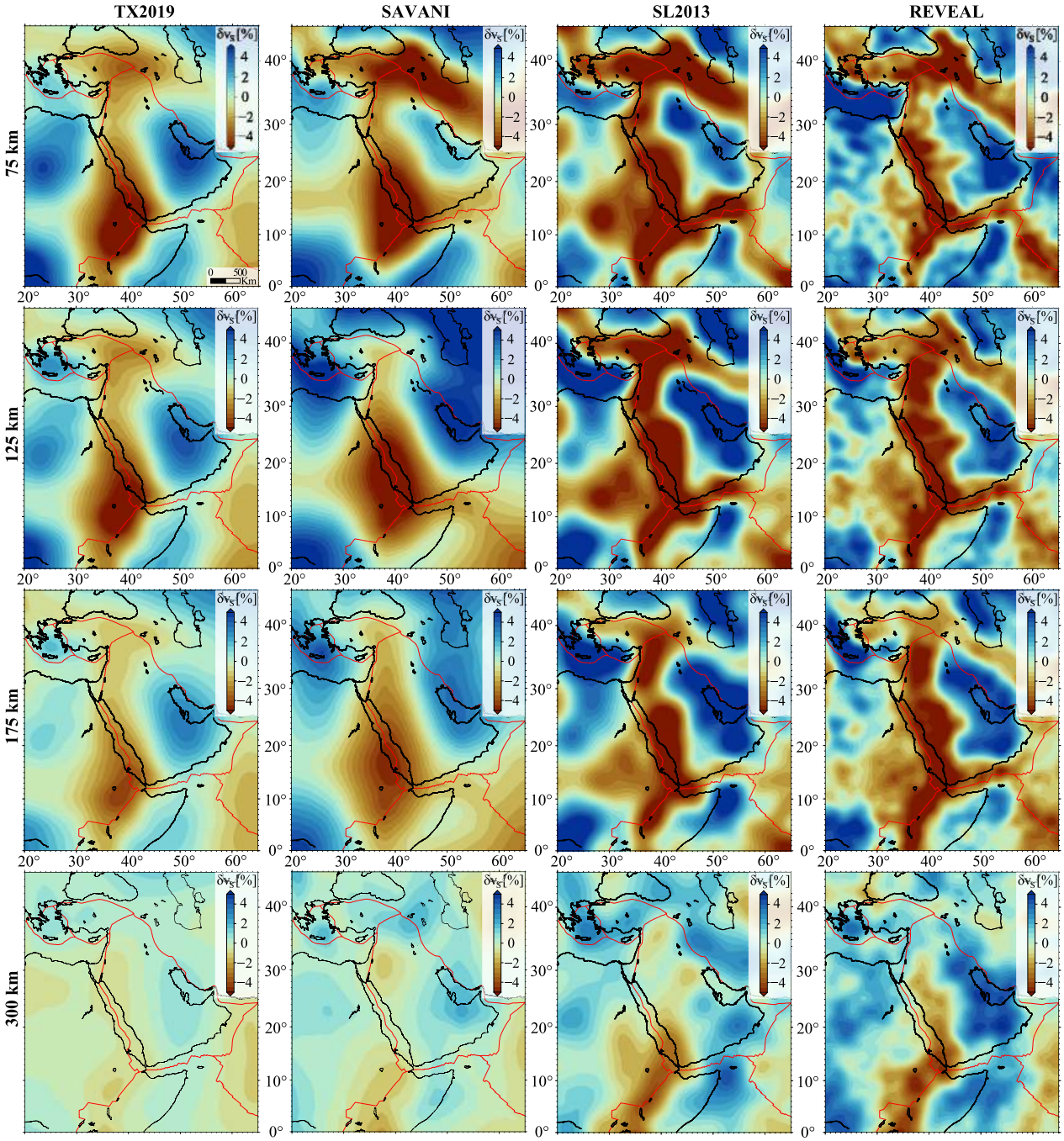

Fig. 2. Comparison of uppermost mantle structure from selected, global shear wave tomographic models: TX2019 (Lu et al., 2019), a body wave model, SAVANI (Auer et al., 2014) a radially anisotropic model based on body and surface waves, SL2013 (Schaeffer and Lebedev, 2013) a surface wave focused, higher resolution SV model, and REVEAL (Thrastarson et al., 2024), a full waveform inversion model. All tomographic models plotted at 75, 125, 175, and 300 km depth. Note the broad region of low seismic velocity below the area comprised between eastern Africa and Levant region. Overall anomalies are consistent across models, with the higher regional resolution models showing consistent northward slow structures, undulating underneath the Arabian plate.

et al., 1989; Camp and Roobol, 1992; Hofmann et al., 1997; Bosworth and Stockli, 2016; Purcell, 2017; Rooney, 2017; Fig. 1). The chemical composition (Baker et al., 1996; Kieffer et al., 2004; Rooney, 2017) and radiogenic isotope ratios (Krienitz et al., 2009; Hua et al., 2023) of the volcanics are consistent with a mantle source with lithospheric contamination.

Several seismic tomography studies show the presence of a broad region of low seismic velocity below the EAAS, interpreted as the signature of hot mantle material (Lithgow-Bertelloni and Silver, 1998; Ritsema et al., 1999; Gurnis et al., 2000; Nyblade et al., 2000; Ritsema and van Heijst, 2000; Benoit et al., 2006a, 2006b; Montagner et al., 2007; Bastow et al., 2008, 2011; Chang and Van der Lee, 2011; Moucha and Forte, 2011; Nyblade, 2011; Faccenna et al., 2013; Hansen and Nyblade, 2013; Schaeffer and Lebedev, 2013; Auer et al., 2014; Emry

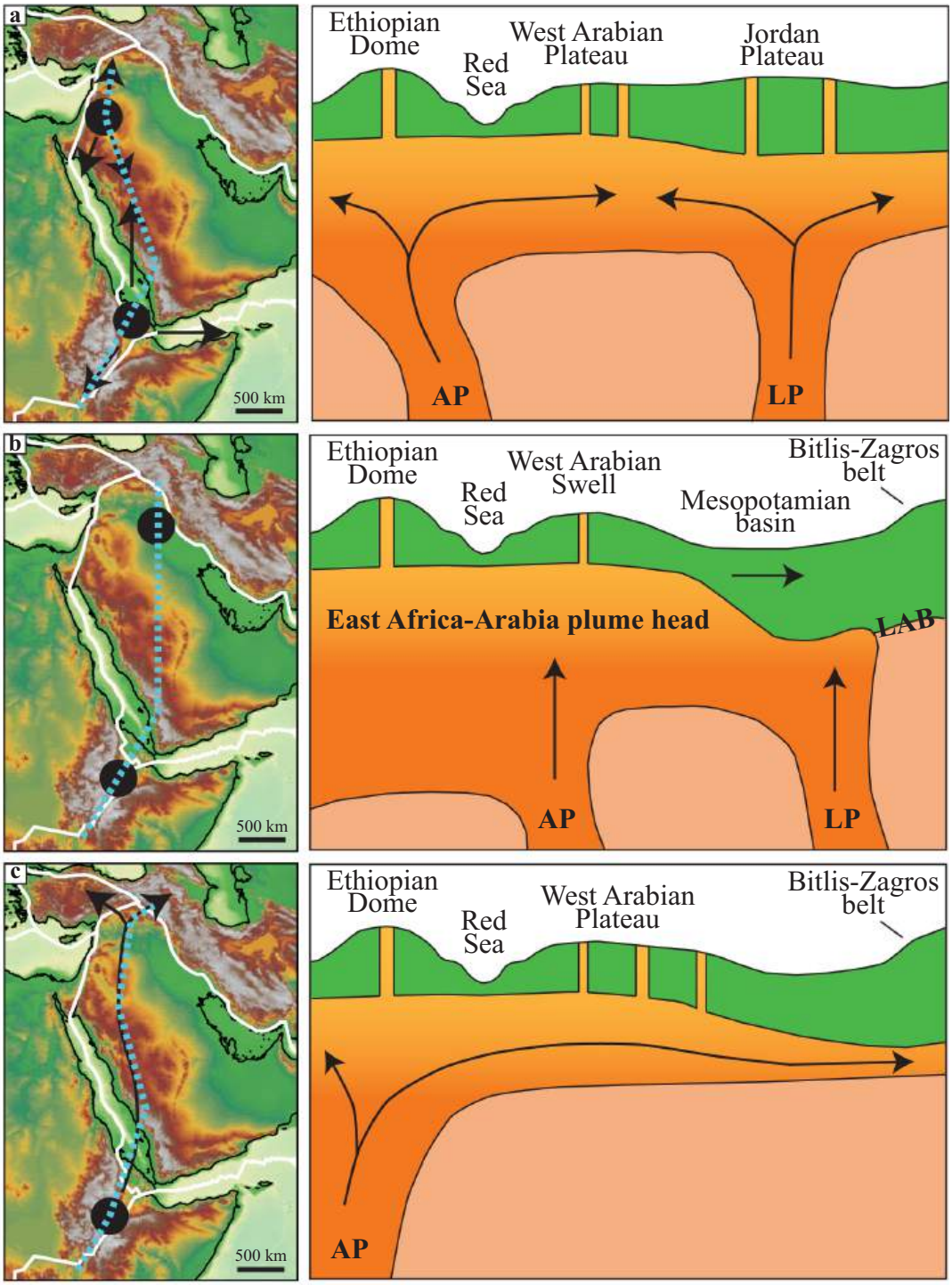

Fig. 3. Schematic maps showing locations of mantle plumes and mantle flow directions (left) with the relative conceptual models (right) according to (a) Chang and Van der Lee (2011), (b) Civiero et al. (2022), and (c) Faccenna et al. (2013). The dashed light blue lines on the maps indicate the traces of the schematic sections represented on the right. AP = Afar Plume; LP = Levant Plume. (For interpretation of the references to colour in this figure legend, the reader is referred to the web version of this article.)

et al., 2019; Lu et al., 2019; Wei et al., 2019; Chang et al., 2020; Tsekhmistrenko et al., 2021; Thrastarson et al., 2024; see Fig. 2). However, although the role of mantle processes has been commonly accepted as the main cause of the current topographic and geologic configurations of the region, in past years there has been debate about the location and number of plumes (Dixon et al., 1989; Ebinger and Sleep, 1998; Chang and Van der Lee, 2011; Hansen et al., 2012; Faccenna et al., 2013; Koulakov et al., 2016). More recent whole-mantle studies (Chang et al., 2020; Tsekhmistrenko et al., 2021; Civiero et al., 2022; Boyce et al., 2021, 2023) seem to converge on the consensus that the region is underlain by a broad low wave velocity anomaly (primarily the African Superplume) with potential addition from other deep-seated plume tails.

In particular, three models can be recognized (Fig. 3). The first indicates the presence of two near-vertical mantle plumes rising below Afar and northern Arabia and flowing beneath the lithosphere (e.g., Debayle et al., 2001; Montagner et al., 2007; Sicilia et al., 2008; Chang and Van der Lee, 2011; Koulakov et al., 2016; Fig. 3a). The second assumes two stationary plumes (Afar and northern Arabia plumes) beneath moving lithospheric plates; in this case, the plume head is stagnating below the lithosphere (e.g., Civiero et al., 2022; Fig. 3b). The last model, in accordance with regional seismic velocity, anisotropy patterns, and seismic tomography (Hansen et al., 2006; Berk Biryol et al., 2011; Schaeffer and Lebedev, 2013; Auer et al., 2014; Qaysi et al., 2018; Lu et al., 2019; Wei et al., 2019; Thrastarson et al., 2024) considers only one mantle plume (Afar superplume) rising below eastern Africa, but flowing to eastern Turkey through pressure gradients and/or prior discontinuities (e.g., Camp and Roobol, 1992; Ebinger and Sleep, 1998; Ershov and Nikishin, 2004; Hansen et al., 2012; Faccenna et al., 2013; Wei et al., 2019; Lim et al., 2020; Agostini et al., 2021; Hua et al., 2023; Fig. 3c).

The uplift pattern of the area is also controversial. In Ethiopia, the uplift is believed to have occurred before (Sengör, 2001), during (Pik et al., 2003), or after (Gani et al., 2007) the emplacement of the volcanic deposits. Some studies (Sembroni et al., 2016a, 2021; Faccenna et al., 2019) suggest that the present topography of Eastern Africa is "a long-term, dynamically supported feature" initiated, at least, in the Oligocene which deeply influenced the present path of the Nile River system (Faccenna et al., 2019). Along the western portion of the Arabian Peninsula, the existence of two distinct groups of volcanic deposits (one dated between 30 and 20 Ma and one younger than 12 Ma), separated by a stasis of few million years in volcanic activity, led Camp and Roobol (1992) to constrain the "initiation of significant uplift", associated with an active mantle upwelling, at the Miocene. Lastly, studies on the topography of the Levant area allowed much of the uplift and the topography to be attributed to the late Oligocene (Avni et al., 2012; Bar et al., 2016).

In this study, we intend to contribute to the discussion about mantle plume number, volcanism, and uplift of the east Africa-Arabia region by analyzing the present surface topographic signal.

Analogue and numerical models produced surface topography related to the impingement of a mantle plume in the form of a long wavelength bulge. While the modeled dynamic topography amplitude scales with asthenospheric density anomalies to first order, the details of geometry and uplift rates depend on mantle–lithosphere interactions, rheological structure, and intraplate stresses (Griffiths and Campbell, 1991; Burov and Gerya, 2014; Kiraly et al., 2015; Sembroni et al., 2017). However, the presence of multiple mantle plumes would suggest a topographic configuration that gives rise to multiple bulges separated by depressed areas. In the case of a single plume locally channelized, the expected surface topography would be characterized by a ridge with the highest elevation at the impingement zone and a gradual decrease to the distal portion.

Therefore, it is not enough to observe the mantle signal to define the geodynamic configuration of a given area. There is a need for the interpretation of that signal to be consistent with the observed surface topographic configuration. To this end we performed a topography analysis (filtered topography, slope, swath profiles) and reevaluated isostatic (flexural isostasy) and dynamic components combining new data with a review of data from literature. Moreover, the pattern of topography along the entire area and the age trend of volcanic deposits of mantle origin have been compared to verify a common trend. The results allow the current topographic configuration of the East Africa-Arabia swell to be attributed to a single mantle plume that, flowing horizontally from East Africa to Turkey, caused uplift and intense volcanism from Eocene to present, influencing the formation and evolution of the major river networks of the area. Much of the present topography is the result of that uplift and of the successive modification by tectonics and surface processes.

2. Geological evolution

The EAAS extends within the Neoproterozoic Arabian Nubian Shield which is split between the Arabian and African plates and extends from Egypt (Sinai Peninsula), through Saudi Arabia, southward to Kenya (Fig. 4). It represents the northern portion of the East African Orogen that formed during the Pan-African Orogeny (900–550 Ma; Stern, 1994) when East and West Gondwana collided to form the supercontinent "Greater Gondwana" or "Pannotia" at the end of Neoproterozoic (Stern, 2002). In the southern part of the shield (Ethiopia and Kenya), the collision produced a pervasive north-trending shear zones; the central-southwestern sections were subjected to oblique and orthogonal east-west compression accompanied by north-south stretching; in the northern and northeastern parts (Arabian Peninsula), shearing and NW-trending thrusting, extension and tectonic escape, resulted in the NW-trending Najd Fault System (Johnson et al., 2017, and references therein).

In the Cambrian, an intensive erosional denudation affected the Arabian-Nubian Shield, forming an extensive low-relief surface over its northern part (e.g., Garfunkel, 1999; Johnson, 2003; Avigad and Gvirtzman, 2009) and in the Horn of Africa (the "pre-Ordovician planation surface" of Coltorti et al., 2007). Between the Precambrian and the Permian, the deposition of sediments at the Gondwana margin formed the Arabian Platform. While the deposits thickened toward the margin of the Arabian Platform, several erosion events exposed the Precambrian basement (e.g., Lebkicher, 1960; Powers et al., 1966; Murris, 1980; Weissbrod and Gvirtzman, 1989; Beydoun, 1991; Kohn et al., 1992; Alsharhan and Nairn, 1995; Ziegler, 2001; Garfunkel, 2002).

During the Permian and Early Mesozoic, continental fragments drifted away and migrated northward, leaving Arabia facing the newly born Neotethys Ocean (e.g., Dercourt et al., 1986; Beydoun, 1991; Alsharhan and Nairn, 1995). In the Horn of Africa this period is characterized by the formation of the Karoo-type rifts and the deposition of 2–4 km of clastic sediments (Beltrandi and Pyre, 1973; Davidson and McGregor, 1976; Davidson, 1983; Hunegnaw et al., 1998; Mège et al., 2015; Macgregor, 2018). Moreover, another denudation event originated a second planation surfaces (the "Late Triassic planation surface" of Coltorti et al., 2007, or the "paleotopography 1" of Sembroni and Molin, 2018) which indicates a pronounced uplift phase (from hundreds of meters to a thousand; see Coltorti et al., 2007). In the Jurassic, after the development of NE–SW and N-S striking structural basins, a main marine transgression took place from S and SE determining the deposition of thick sequences of marine marls, limestones, and evaporites (Guiraud et al., 2005; Davison and Steel, 2018; Macgregor, 2018). Since the Lower Jurassic, the extensional deformation caused the separation of the Madagascar-India block from Eastern Gondwana (Reeves and De Wit, 2000; Seward et al., 2004; Gibbons et al., 2013; Gaina et al., 2015; Macgregor, 2018). During the Late Cretaceous, the closure of the Neotethys Ocean (e.g., Robertson and Dixon, 1984; Garfunkel, 1998, 2004; Robertson et al., 2006) resulted in a horizontal compression and the formation of the S-shaped Syrian Arc fold belt, extending from Sinai to

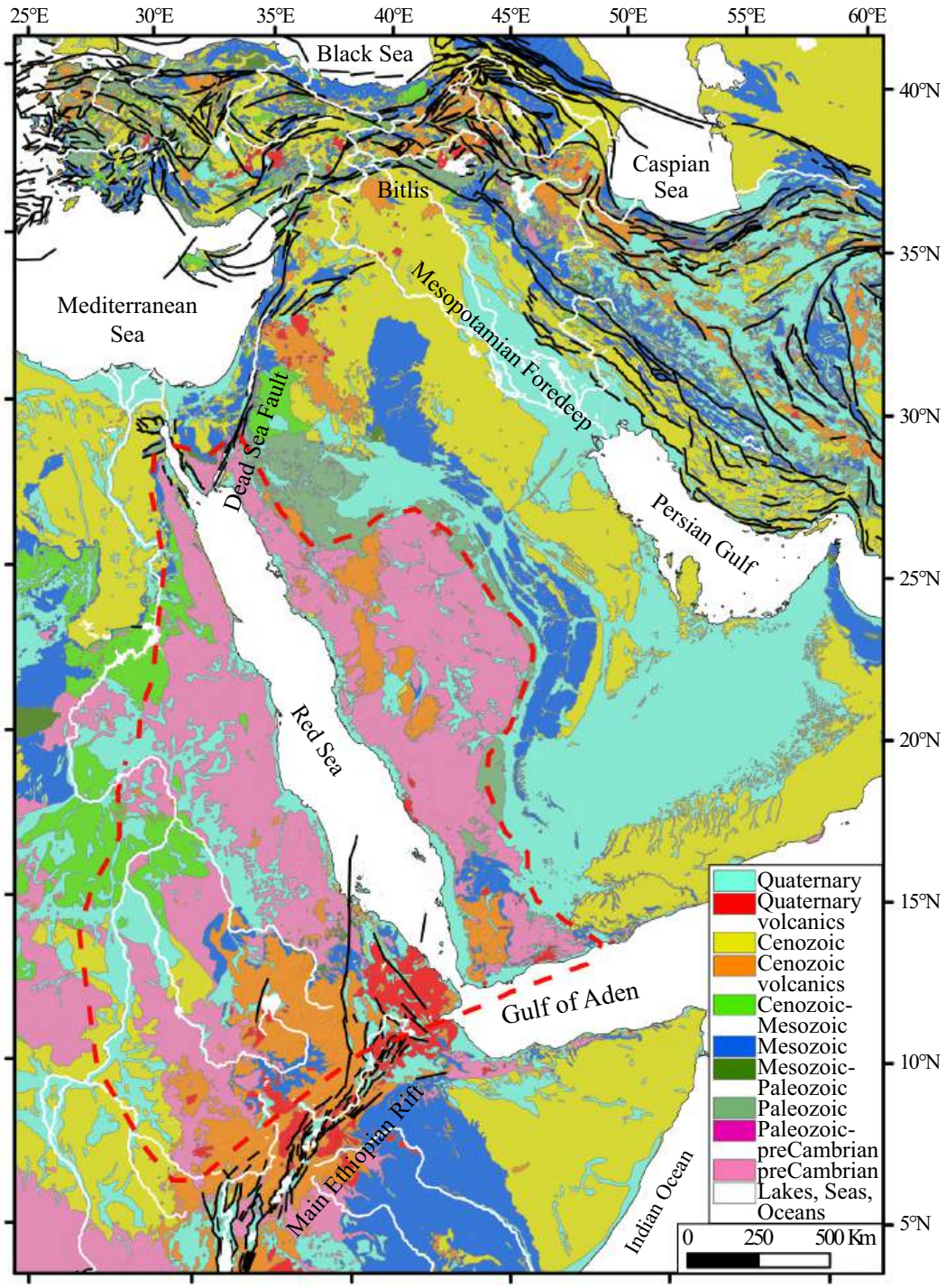

Fig. 4. Geological map of the study area (modified from the Lithologic Map of the World; (Hartmann and Moosdorf, 2012); active tectonic lineaments (solid black lines) are from the Global Active Faults database by Styron and Pagani (2020); dashed red line contours the Arabian-Nubian Shield (from Alemu, 2021). (For interpretation of the references to colour in this figure legend, the reader is referred to the web version of this article.)

Syria where it is represented by the Palmyride inversion zone and fold belt (Krenkel, 1924; Chaimov et al., 1990; Brew et al., 2001), while in eastern Africa a new extensional tectonic phase formed several NW-SE narrow basins and a third denudation event originated the "Cretaceous planation surface" (Coltorti et al., 2007), "paleotopography 2" of Sembroni and Molin (2018). At the end of the middle Eocene the most extensive transgression over the Arabian Platform terminated (Ziegler, 2001; Gvirtzman et al., 2011; Avni et al., 2012). In the same period the separation of Arabia from Africa (6–13 mm/yr; Sella et al., 2002; McClusky et al., 2003; Reilinger et al., 2006; Vigny et al., 2006; ArRajehi et al., 2010) occurred along with the development of the Gulf of Aden and Red Sea rift systems (Bosworth et al., 2005; Leroy et al., 2012). Continental rifting at the Gulf of Aden initiated between 38 and 33 Ma (Pik et al., 2013; Robinet et al., 2013; Purcell, 2017; Boone et al., 2021), concurrently with the onset of the Arabia-Eurasia collision (~23 mm/yr; ArRajehi et al., 2010; McClusky et al., 2003; Reilinger et al., 2006; Sella et al., 2002; Vigny et al., 2006). Thermochronology data indicate that collision took place at ~20 Ma along the Bitlis-Zagros zone (Okay et al.,

2010), though older ages have been proposed (Pirouz et al., 2017; Koshnaw et al., 2019).

During the Oligocene, geological and thermochronological data indicate a pronounced phase of uplift both in Ethiopia (Sengör, 2001; Pik et al., 2003; Sembroni et al., 2016a, 2016b; Sembroni et al., 2021) and along the Arabian plate (Gvirtzman et al., 2008; Avni et al., 2012; Bar et al., 2013; Turab et al., 2023), where the marine environments shifted toward the margins (e.g., Beydoun, 1991; Alsharhan and Nairn, 1995; Ziegler, 2001). The Arabian inland region and eastern Africa were subjected to denudation, which led to the formation of extensive low-relief surfaces (e.g., Lebkicher, 1960; Alsharhan and Nairn, 1995; Burke and Gunnell, 2008; Avni et al., 2012; Bar et al., 2016) termed "the Oligocene Peneplain" in northern Arabia (Picard, 1951; Quennell, 1958; Garfunkel and Horowitz, 1966; Avni, 1991; Zilberman, 1991; Avni et al., 2012; Zilberman and Calvo, 2013; Bar et al., 2016) and "Trap volcanics planation surface" (Coltorti et al., 2007) or "paleotopography 3" (Sembroni and Molin, 2018) in eastern Africa.

At ~27 Ma, rifting commenced along the western and southern Afar margins (Purcell, 2017). The western Afar faulting marks a continuation of the Red Sea rifting which, in the meanwhile, was opening starting from its southern portion (Bosworth et al., 2005; Wolfenden et al., 2005; Purcell, 2017; Boone et al., 2021). At the beginning of Miocene, the East African Rift (EAR) started the expansion both north and south from the Turkana region (Purcell, 2017).

Between 18 and 14 Ma, the Arabian plate separated from the Sinai sub-plate by the ~1000 km long Dead Sea Transform Fault (DSTF; Quennell, 1958; Freund et al., 1970; Garfunkel, 1981; Garfunkel et al., 1981; Joffe and Garfunkel, 1987; Bosworth et al., 2005) and began rotating counterclockwise. Recent dating of *syn*-faulting calcite has further constrained the formation of the DSTF plate boundary to 20.8–18.5 Ma in southern Israel and propagating northwards by 17.1 Ma (Nuriel et al., 2017). At the northern boundary of the Arabian Plate, the stress regime appears to have changed from compressional to strike slip, due to the oblique collision between Anatolian and Arabian plates (e.g., Beydoun, 1999). This caused the lateral escape of the Anatolian Plate, accommodated by a system of lithospheric scale dextral (North Anatolian Fault) and sinistral (East Anatolian Fault) strike slip faults (Şengör et al., 2005; Reilinger et al., 2006; Ballato et al., 2018). At ~13 Ma the EAR tectonic activity increased: the Western Branch and the northern segment of the Main Ethiopian Rift (MER) started to form (Macgregor, 2015; Purcell, 2017).

The central portion of the MER started joining the southern and northern segments between 8 and 5 Ma (Bonini et al., 2005; Abebe et al., 2010). In the Pleistocene, the deformation and the main magmatic activity abandoned the MER margin faults and shifted to the floor of the rift valley with the formation of the oblique Wonji Fault Belt (Ebinger, 2005; Corti, 2009; Purcell, 2017).

From the middle-late Miocene, to the north of the Bitlis collision zone, the Eastern Anatolian Plateau experienced a strong exhumation, probably due to the combined effects of a more advanced stage of the Arabia-Eurasia collision (Okay et al., 2010; Ballato et al., 2011; Cavazza et al., 2018, 2019; Gusmeo et al., 2021; Darin and Umhoefer, 2022) and the arrival of hot mantle material below the lithosphere (Molin et al., 2023, and references therein).

Plate reconstructions and geodetic data suggest that the present-day motion of the Arabian plate relative to the Nubian and the Eurasian plates stayed consistent since at least 11 Ma (e.g., ArRajehi et al., 2010; McClusky et al., 2010; Reilinger and McClusky, 2011; Viltres et al., 2022).

2.1. Volcanism

Intra-plate basaltic volcanism started in southern Ethiopia/northern Turkana at 46 Ma ("Eocene Initial Phase" of Rooney, 2017) and lasted for ~10 Ma. After a short hiatus, new basaltic eruptions ("Oligocene Trap phase"; Rooney, 2017) covered parts of Ethiopia, Eritrea, southern Sudan, and western Yemen by 30–29 Ma (Hofmann et al., 1997; Fig. 4). This period of volcanism was coeval with initial faulting and deposition of syn-rift strata in the Gulf of Aden (Purcell, 2017; Rooney, 2017). In the same period, an intense magmatic activity occurred along the Western Arabian margin exploiting the NW-SE discontinuities associated with the Precambrian Najd Fault System ("Older Harrats"; Bosworth and Stockli, 2016; Fig. 4). Subsequently, a period of relative magmatic quiescence took place in the Horn of Africa with volcanism mainly concentrated in the Turkana area (Ukstins Peate and Bryan, 2008; Brown and Mcdougall, 2011), along the rift margins in Ethiopia and Yemen (Rooney et al., 2013), and in eastern Ogaden (Mège et al., 2016; Sembroni and Molin, 2018).

This period of volcanic quiescence is reflected in Ethiopia by the deposition of voluminous intratrappean sediments composed of red clays and sands between 29 and 27 Ma (Abbate et al., 2014). The last eruptions of the continental flood volcanics occurred at 26.5 Ma in Yemen and 25 Ma in Ethiopia. At 24 Ma basaltic dikes and igneous complexes formed northwest of Afar and along the present-day Red Sea margin of Yemen and Saudi Arabia (e.g., Coleman et al., 1983; Brown et al., 1989; Camp and Roobol, 1992; Ilani et al., 2001; Trifonov et al., 2011). At the same time, a large basaltic volcanic province developed in northern Egypt and in the Harrat Ash Shaam region of Jordan, while extensive NW-SE-trending diking, granitic intrusions and silicic volcanism occurred along the 1700 km length of the Western Arabian margin (Fig. 4).

In the middle-late Miocene voluminous volcanism affected the Eastern Anatolian Plateau (Keskin, 2003) causing the covering of large portion of the forming plateau (Fig. 4). This event seems to be coeval with both the collisional deformation along the Bitlis suture zone and the formation of the northern and eastern Anatolian faults (e.g. Keskin, 2003; Şengör et al., 2003; Faccenna et al., 2006; Faccenna et al., 2013; Schildgen et al., 2014; Memiş et al., 2020). In the same period (~13 Ma) a renewed magmatic phase, associated with the N-S movement along the DSTF, affected the Arabian Shield with the eruption of the so-called "Younger Harrats" (Bosworth and Stockli, 2016). Once initiated, volcanism at most locations continued until present.

3. Geomorphological setting

The East Africa-Arabia region displays spectacular signs of an ongoing mantle-plume impact on its surface. One of the most evident is the EAAS which extends for ~4000 km from Jordan to Ethiopia and ~1500 km from east to west (Almond, 1986; Dixon et al., 1989; Camp and Roobol, 1992; Fig. 1). To the south, the NW-SE trending Turkana depression, developed in the Early Cretaceous, separates the swell from the Kenya dome, while to the north the NW-SE trending Mesopotamian basin stands between the swell and the Bitlis Mts. (Fig. 4). While the low-lying nature of the Turkana region is the result of crustal stretching during the end of Mesozoic and Cenozoic (Kounoudis et al., 2023; Ogden and Bastow, 2022), the Mesopotamian lowland represents what remains of the foreland basin of the Zagros Fold and Thrust Belt and is ~900 km long and ~200 km wide (Berberian, 1995; Hessami et al., 2001).

Several studies demonstrated the presence of paleosurfaces both in the Arabia Peninsula (Avni et al., 2012; Bar et al., 2016) and in the Horn of Africa (Coltorti et al., 2007, 2015; Gani et al., 2007; Sembroni et al., 2016a; Sembroni and Molin, 2018; Sembroni et al., 2021). Avni et al. (2012) documented a regional truncation surface outcropping in the northern portion of the Red Sea and in the southern Levant region which separate middle Eocene – early Oligocene pre-rift deposits from late Oligocene – Holocene conglomerates and volcanic rocks. For this reason, the authors referred this surface to the Oligocene. Bar et al. (2016) extended such a surface to the western half of the Arabia Peninsula and defined it as a planation surface standing at elevation ranging between 800 and 1200 m (Arabian Plateau in Fig. 1). To the west and south, the Arabian Plateau is bounded by the elevated shoulders of the Red Sea and the Gulf of Aden rifts. To the north and east the plateau gently descends

toward the Persian Gulf and the Mesopotamian Basin. The northeastern portion of the Arabian Plateau comprises the Jordan Plateau, a large eastward-tilted area with summits at 1200–1700 m and elevation increasing southward (Fig. 1). The evolution of this structure seems to be linked to the formation of the Dead Sea depression (Salameh, 1997; Avni et al., 2012; Bar and Zilberman, 2016; Ben-Israel et al., 2020).

Similarly, at the opposite side of the Red Sea, the Horn of Africa presents remnant surfaces representing the preserved top of the basaltic plateau formed after huge eruptions occurred mainly in the Oligocene Trap phase (the "Trap volcanics planation surface" of Coltorti et al., 2007, or "paleotopography PT3" of Sembroni and Molin, 2018). These sub-horizontal (< 3°) surfaces stand at an elevation comprised between 1000 m (in southern Ethiopia) and 2700 m (in central and northern Ethiopia; Sembroni et al., 2016a, 2016b) forming the so-called Ethiopian-Somalian Plateau (Fig. 1). This plateau is divided into the Ethiopian and Somalian portions by the NE-SW trending MER. Locally, large shield volcanoes rise 1000–2000 m above the average plateau elevation, the highest of which reach elevations >4200 m. The Ethiopian Plateau consists of a flat to gently rolling landscape (Fig. 1). Conversely the Somalian Plateau is much less extensive and presents the flat top along the southeastern margin of the MER (Fig. 1). To the west and southeast of the high elevated plateaux, the topography gradually decreases down to 500 m respectively in the Sudan and Somalian lowlands (Fig. 1). According to several studies the incision of these uplands initiated by regional uplift in the Late Oligocene continuing up to present time (McDougall et al., 1975; Pik et al., 2003; Gani et al., 2007; Ismail and Abdelsalam, 2012; Gani, 2015; Sembroni et al., 2016b; Gani and Neupane, 2018; Sembroni and Molin, 2018; Sembroni et al., 2021; Gani et al., 2023). This long-lasting incision sculpted a landscape characterized by steep slopes bordering high-elevated low relief surfaces underlain by continental flood basalts (plateau remnants; Sembroni et al., 2016b).

The Ethiopian-Somalian and Arabian plateaux are separated by the NW-SE trending Red Sea which displays longitudinal and along-strike variations in rift flank morphology (Fig. 1). In particular, the western margin is characterized by the narrow, 1500 km long "Red Sea Hills" (mean elevation 500 m), while the conjugate Arabian escarpment presents highlands averaging 1000–1500 m in elevation.

Immediately to the north of the Mesopotamian basin, the East Anatolia Plateau consists of a dome-shaped feature characterized by a rolling low-relief topography standing at a mean elevation of ~2000 m (Molin et al., 2023; Fig. 1). Volcanoes rise from its surface, some of which reach 5000 m. To the north and south, the topography decreases down to sea level.

The hydrography of these high elevated region shows a typical radial pattern both in Ethiopia (Nile drainage system; Sembroni et al., 2021) and in Arabia (Fig. 1). An exception is the Eastern Anatolian Plateau where rivers integrate into the plateau in a disorganized way, locally following tectonic structures (i.e., the Euphrates River; Molin et al., 2023; Fig. 1).

4. Deep mantle processes beneath East Africa - Arabia

Uplift, rifting, and volcanism in the East Africa-Arabia region have been related to one or more plumes, based on geochemical, seismic, and other evidence (Ebinger et al., 1989; Camp and Roobol, 1992; Burke, 1996; Ebinger and Sleep, 1998; Courtillot et al., 1999; Rogers et al., 2000; Montelli et al., 2006; Rogers, 2006; Chang and Van der Lee, 2011; Fishwick and Bastow, 2011; Nelson et al., 2012; Chang et al., 2020; Civiero et al., 2022). Thin-lithosphere corridors have been proposed to assist in plume transport or channel plume material to volcanic fields hundreds of kilometers away (cf. Fig. 2; Camp and Roobol, 1992; Ebinger and Sleep, 1998; Faccenna et al., 2013; Agostini et al., 2021; Civiero et al., 2022; Hua et al., 2023).

The strongest geochemical evidence for the presence of plume material below the region is the lack of a prominent contribution from shallow, depleted MORB mantle in the source material for pre-rift volcanism (Baker et al., 1996; Kieffer et al., 2004). Isotopic measurements in the basalts of southern Ethiopia, Afar, and Levant all indicate deep-mantle reservoirs, with a lithospheric component (e.g., Krienitz et al., 2009; Nelson et al., 2012).

Recently, Hua et al. (2023), according to a wide range of seismic and geochemical observations, inferred that the hot asthenosphere beneath Anatolia is fed by long-distance lateral transport of upper mantle from East Africa, with the lateral flow being driven by pressure gradients created by the buoyancy of the African mantle plume, consistent with the earlier inferences of Ershov and Nikishin (2004) and the mantle flow and seismic anisotropy modeling of Faccenna et al. (2013) (Figs. 2 and 5). In agreement with the suggested progressive northward motion of asthenopsheric plume material, seismic body and surface wave imaging (Fig. 2) and seismic anisotropy of the upper mantle, e.g. as inferred from SKS splitting (Fig. 5) beneath East Africa and Arabia appear related to the combination of channelized flow from Afar along the Red Sea (e.g., Hansen et al., 2012; Bagley and Nyblade, 2013; Faccenna et al., 2013; Hammond et al., 2014; Wei et al., 2019), and oriented partial melt pockets of other rifting associated processed closer to the Ethiopian flood basalt province (e.g., Kendall et al., 2005; Bastow et al., 2010; Ebinger et al., 2024).

The associated low-velocity anomaly crosses the upper mantle under East Africa and continues propagating northeasterly to western Arabia (Figs. 2 and 5). Some tomography models show a low-velocity feature in the upper mantle extending from the Red Sea into the interior of Arabia (Debayle et al., 2001; Benoit et al., 2006a, 2006b; Fishwick, 2010; Emry et al., 2019) and a narrow anomaly aligned with the Red Sea but offset to the east (Chang and Van der Lee, 2011; Chang et al., 2011; Koulakov et al., 2016; Lim et al., 2020; Tang et al., 2018; Yao et al., 2017). In contrast, Civiero et al. (2022) proposed three mantle plumes beneath Kenya, Afar, and Levant feeding an integral East Africa-Arabia plume head. Low shear-wave velocities beneath the Gulf of Aden down to 150 km depth were also reported, suggesting that the plume below Afar may be also feeding the Gulf of Aden ridge (Sicilia et al., 2008).

If we assume that seismic anisotropy is due to shear in mantle flow, the updated SKS compilation of Fig. 5 is consistent with previous discussions about plume-related, and slab curtain modulated, asthenospheric channeling, and in particular the mantle flow and texture formation modeling of a more limited SKS dataset by Faccenna et al. (2013). However, the more extensive coverage of the Arabian Peninsula provides an opportunity to further explore details of channeling and deflection of flow by lithospheric structure, for example.

5. Methods and results

To describe the extension and geometry of the EAAS and to investigate the different components of topography, the present topographic configuration of the study area has been analyzed by several techniques including slope map, swath profiles, and filtered topography. To quantify the isostatic component of topography along the Red Sea rift shoulders, the flexural uplift has been calculated. The non-isostatic contribution to topography has been quantified by the realization of residual and dynamic topography maps. As elevation data source we used the ETOPO2022 global elevation model (resolution of 15 arc-second = ~500 m; www.ngdc.noaa.gov) because its relative fine resolution allows the analysis of topography at a regional scale. The data have been extracted and elaborated by means of ArcGIS and MatLab software.

To highlight a possible common trend between topography and volcanism age patterns, topography analysis results have been analyzed together with geochronological data. In detail, 1465 published ages of volcanic deposits from Ethiopia to Turkey have been collected and statistically analyzed.

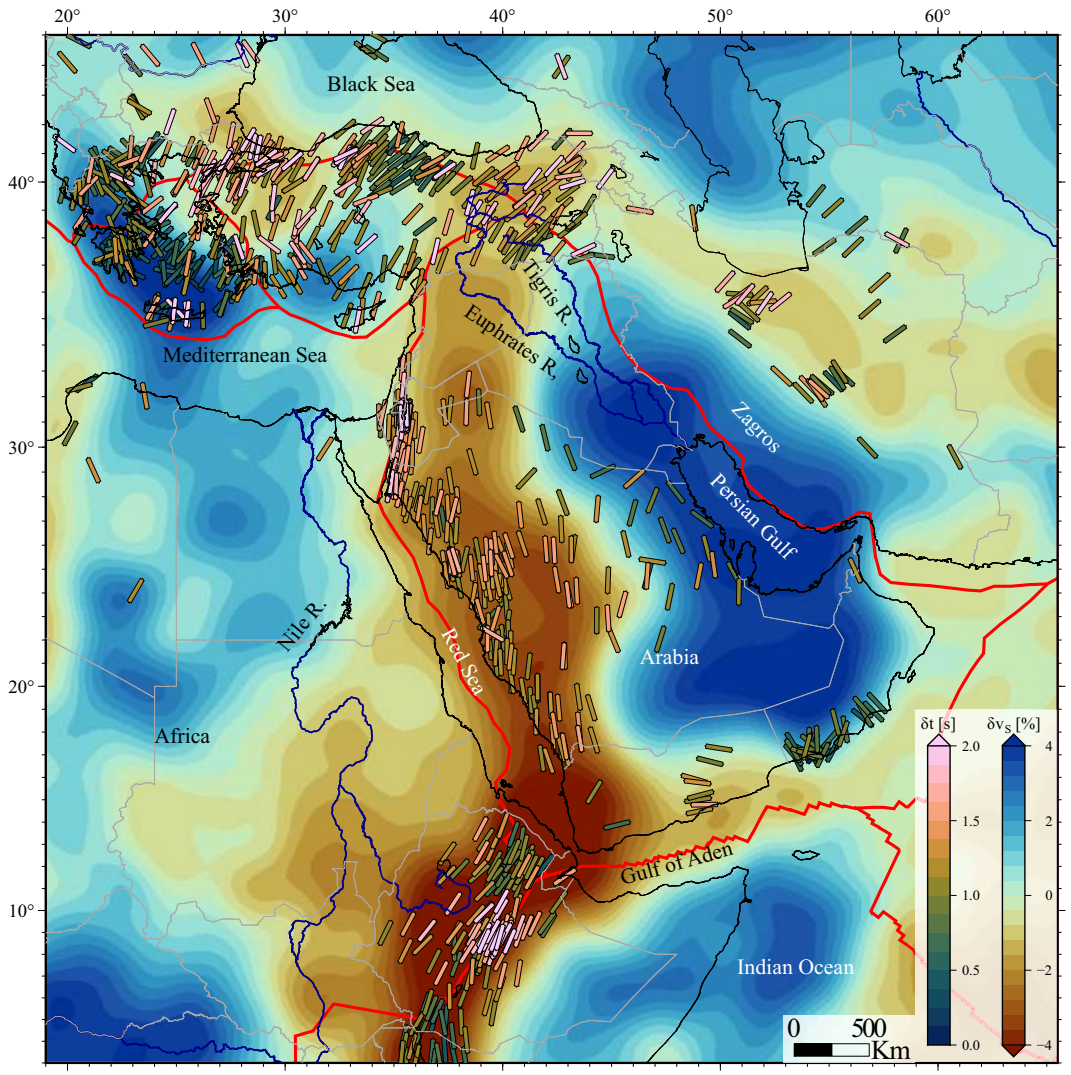

Fig. 5. REVEAL tomography model (Thrastarson et al., 2024) (see Fig. 2) averaged over the 100…400 km depth range (which dominates dynamic topography, cf. Fig. 10f) superimposed by SKS splitting observations aligned with "fast axes" and colored by delay time (compilation of Becker et al., 2012, updated as of 05/2024). Solid black show coastline, blue lines major rivers, and red line major plate boundaries. (For interpretation of the references to colour in this figure legend, the reader is referred to the web version of this article.)

5.1. *Slope map and filtered topographies*

Slope maps have been widely used to mark morphologies, such as high-standing plateaux or steep escarpments, which are not immediately detectable from the observation of a DEM. In this study, a slope map from the ETOPO2022 DEM has been generated in ArcGIS environment by the "Slope" tool which identifies the variation in elevation over the distance (3 × 3 cell neighborhood) for each cell of the DEM. The tool, interpolating the gradient value of cell centers, generates a plane whose slope value is calculated using the average maximum technique (Burrough and McDonnell, 1998). In this study the values have been classified in four classes (Fig. 6): the first three classes describe flat or gently dipping portions of landscape with slope <15°; the last class covers the range 15°-69° to emphasize escarpments.

The map shows the highest slope values (> 15°) in coincidence with the margins of the Red Sea, the Afar and MER escarpments, along the DSTF, and in the mountainous regions in the southernmost (Ethiopia) and northernmost (Turkey, Armenia, Azerbaijan, Iran) portions of the study area (Fig. 6). The lowest values (< 5°) concentrate on the remaining part and differentiate into low-elevated and high-elevated areas. The former ones correspond to the Nile, Tigris and Euphrates rivers valleys, the Persian Gulf surroundings, and the Horn of Africa coastal zone. Conversely, the high-elevated sub-horizontal surfaces are in the inner sectors of Turkey (Anatolian Plateau) and Iran (Iranian Plateau), along the western margin of the Arabian Peninsula (Arabian Plateau), and in the Ethiopia (Ethiopian-Somalian Plateau).

Previous studies on the region (Almond, 1986; Dixon et al., 1989; Camp and Roobol, 1992; Sengör, 2001; Şengör et al., 2003; Forte et al., 2010; Faccenna et al., 2013; Sembroni et al., 2016a, 2016b, 2021) relate large-scale morphologies to mantle processes. To isolate and quantify this component, the present topography of the study area has been filtered in frequency domain by a circular low pass filter in ArcGIS environment. This methodology has been used in other parts of the world such as Yellowstone and Colorado Plateau (Wegmann et al., 2007; Roy et al., 2009), Eastern Africa (Sembroni et al., 2016b, 2021), Apennines and Carpathians (D'Agostino and McKenzie, 1999; Molin et al., 2004, 2012; Faccenna et al., 2011), and Easter Anatolia Plateau (Molin et al., 2023). To avoid flexural effects, the choice of the filter wavelength is important (Molin et al., 2012). In this study we used two wavelengths: 200 (Fig. 7a) and 400 km (Fig. 7b). Such values are effective in filtering out the topographic signals of crustal tectonics and fluvial wide valleys and to isolate the mantle component (D'Agostino and McKenzie, 1999; Molin et al., 2004, 2012; Wegmann et al., 2007; Roy et al., 2009; Faccenna et al., 2011; Sembroni et al., 2016b, 2021). In particular, the

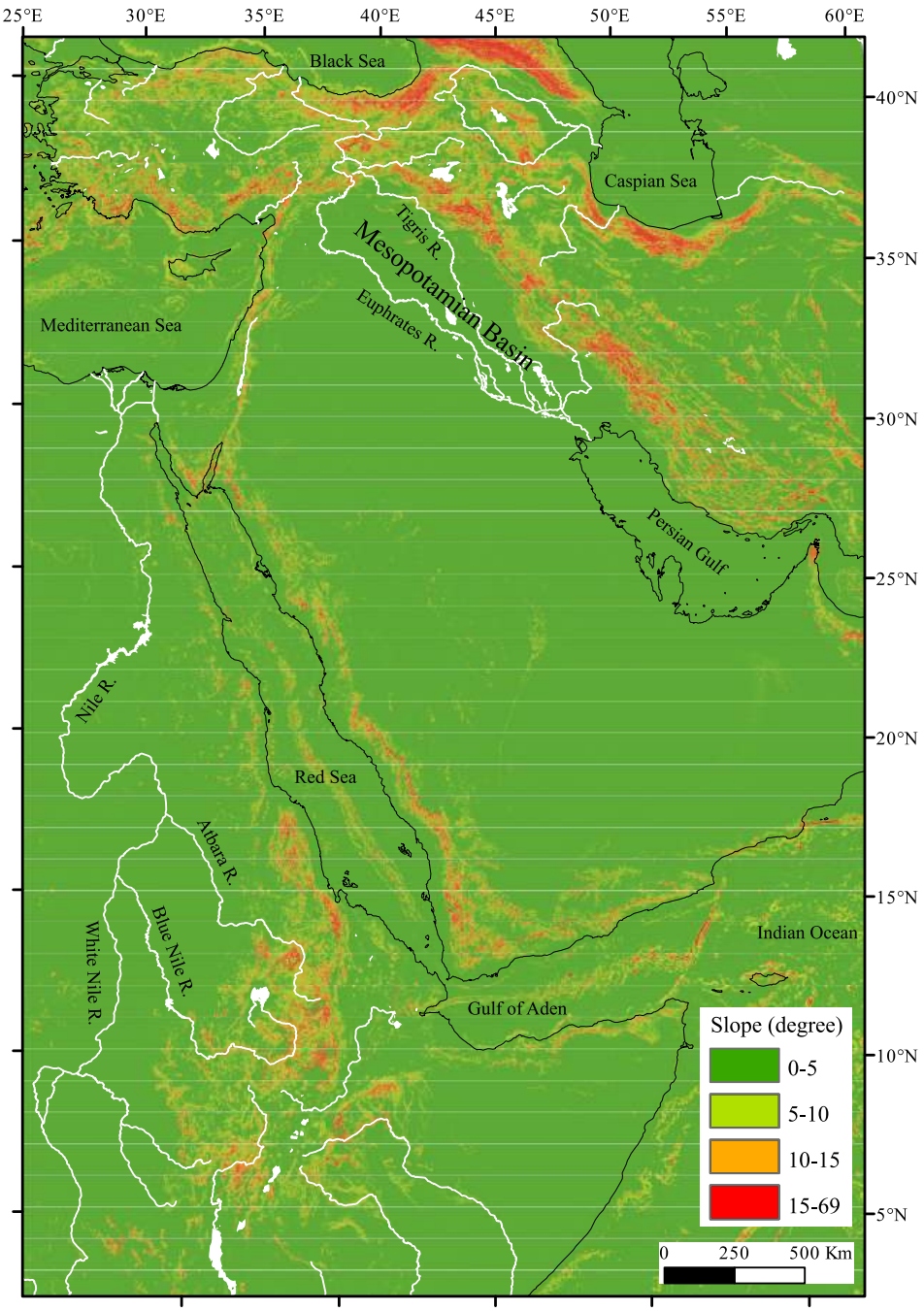

Fig. 6. Slope map of the study area elaborated from the ETOPO2022 global elevation model.

wavelength at 400 km allows to inhibit the topographic influence of the Red Sea, which presents a maximum width of ~300 km, and to discern the deeper component of the topography.

In the filtered topography at 200 km wavelength (Fig. 7a), values between 500 and 1000 m characterize a long strip of land from Ethiopia to Syria (NNW-SSE trend) interrupted only in coincidence with the Red Sea and the Gulf of Aden. Indeed, their maximum amplitude of 300 km exceeds the radius chosen for filtering the topography. We referred this topographic feature to the EAAS. Its highest elevation (1000–2500 m) falls in the Ethiopian-Somalian Plateau and in the southwestern corner of the Arabia peninsula. The swell is bordered to the west and east by lowlands at elevation comprised between 0 and 500 m represented, respectively, by the Nile River Valley and by the Mesopotamian Basin – Persian Gulf area. To the north, the filtered topography slightly decreases in northern Syria and then dramatically increases up to 2500 m in coincidence with the Anatolian Plateau and the Zagros Mts.

In the 400 km filtered topography (Fig. 7b), the swell is still clearly visible presenting almost the same elevation pattern and geometry previously described. In this case the higher elevation (1000–2000 m) focuses exclusively on the Horn of Africa while the Arabian Peninsula shows a relatively homogeneous elevation between 500 and 1000 m.

5.2. *Swath profiles*

A swath profile is a distance vs. elevation plot in which the trend of maximum, minimum, and mean topography is represented within a specific rectangular observation window (swath). Swath analysis has been widely used to compare magnitudes of orogenic belts (Fielding,